Jurnal Fizik Malaysia Volume 43 Issue 1 (2022) pgs 10201-10213 M. S. Abdullah

Nuclear Properties of Og-isotopes within the Skyrme Mean-Field Approach

Mastura Syamimi Abdullah[a] and Meng-Hock Koh[a,b]

[a]*Department of Physics, Faculty of Science, Universiti Teknologi Malaysia, 81310 Johor Bahru, Malaysia*
[b]*UTM Centre for Industrial and Applied Mathematics, Ibnu Sina Institute for Scientific and Industrial Research, Universiti Teknologi Malaysia*

(Received: 1.11.21 ; Published: 24.9.22)

Abstract. In this work, we present results of potential energy surfaces, two-neutron separation energies and its energy differential of Og- and Lv-isotopes, as well as the alpha-decay half-lives of the Og-isotopes. Calculations were performed using the Skyrme-Hartree-Fock-plus-Bardeen-Cooper-Schrieffer (SHF+BCS) approach. We found that the potential energy surfaces and two-neutron separation energy differential indicated that $N = 184$ is a candidate for the next neutron magic number after $N = 126$, as is already well known. However, the alpha-decay half-lives calculated with different semi-empirical formulas showed a higher stability for its neighbouring $N = 182$ and $N = 180$ nuclei. We have also made a test on the choice of pairing strengths by comparing results obtained using a fixed pairing strengths determined from previous study in the actinide region, and the set of pairing strengths adjusted to reproduce the Madland pairing gap for the ^{294}Og nucleus. We found that the pairing strengths adjusted to the Madland pairing gap gives a half-life close to the upper limit of the experimental data when using the Brown, modified Brown and Royer semi-empirical formulas.

Keywords: Superheavy nuclei, Hartree-Fock, Skyrme, Bardeen-Cooper-Schrieffer, magic numbers

INTRODUCTION

Discovery of new superheavy elements in the last two decades [1] marks an important and exciting moment for the nuclear physics community. The motivation for experimentalists and theorists working in the superheavy region is to locate the so-called island of stability. The island of stability is made up of nuclei which are relatively more stable due the existence of nuclear magic numbers. It is well known that nucleon number 2, 8, 20, 28, 50, 82 and 126 form the spherical magic numbers. Nucleus having magic number is special due to it having longer half-life and hence more stable as compared to its neighbouring nuclei [2]. The heaviest doubly magic nucleus ^{208}Pb consists of 82 protons and 126 neutrons. However, the element with $Z = 126$ has yet to be synthesized in the laboratory. The heaviest element synthesized in the laboratory is $Z = 118$ with a half-life of 0.6 μs [3] which is extremely short. On the theoretical side, there are now a significant increase in studies in this nuclear region. One example of the previous work is on the prediction of the nuclear shape [4] while other studies deal with prediction of spontaneous fission and alpha decay half-life [5-9].

Paper contributed to the National Physics Conference 2021 (PERFIK2021), 29 – 30 June 2021

As experimentalists try to uncover the journey of so-called island of stability, the theorists are helping by making the prediction of the possible next nuclear magic numbers. There are two types of approaches that have been used to predict the nuclear magic number which namely those based on microscopic approach utilizing a phenomenological internucleon interaction [10] and those based on the macroscopic-microscopic approach such as the liquid drop model (LDM) plus Strutinski shell correction method [11]. Studies based on the microscopic approaches have predicted N = 172 [12] and 184 [12-14] as the next neutron magic numbers and Z = 114 [12-14], 120 [12,14], 122[14] and 126 [12,14] as the next proton magic numbers. Contrary to that, macroscopic-microscopic approaches predicted N = 162 [15], 172[16] and 184 [16,17] as the next neutron magic numbers and Z = 108 [15],114 [17], 120[16], 124 [16], 126 [16] as the next proton magic numbers. All of these reflects that the journey to uncover the next nuclear magic numbers around superheavy region is far from being solved. Different approaches and different observables give different prediction on nuclear magic number. Therefore, we are interested to identify magic numbers in superheavy region by investigating various physical quantities such as quadrupole moments (Q_{20}), two-neutron separation energies and its differential and alpha decay half-lives of Og-isotopes with several formulas within Skyrme Hartree-Fock-plus-Bardeen-Cooper-Schrieffer (HF+BCS) approach.

In this paper, we report some preliminary results on the potential energy surface, alpha-decay half-life and two-nucleon separation energies based on the Skyrme HF+BCS approach. The manuscript is arranged such that we discussed the theoretical framework covering the Skyrme HF + BCS, two-neutron separation energy and its differential and the semi-empirical formulas for alpha-decay half-life in Section 2. This is followed by some technical details of our calculations in the Section 3. We then present our results in Section 4 and the concluding remark in Section 5.

THEORETICAL FRAMEWORK

Skyrme Hartree-Fock-plus-Bardeen-Cooper-Schrieffer (HF+BCS)

General Hamiltonian can be written as

$$\hat{H} = \sum_i \hat{K}_i + \frac{1}{2}\sum_{ij} \hat{V}_{ij} \tag{1}$$

where $\hat{K}_i$ is the kinetic energy operator and $\hat{V}_{ij}$ is the two-body interaction. However, in nuclear physics field, there is no known exact potential. Therefore, in this study, $\hat{V}_{ij}$ is assumed as Skyrme interaction [18]. In the Independent Particle Model (IPM), the particles are assumed to be moved independently with one another. So, one-body interaction is introduced in Eq. (1) and can be written as

$$\hat{H} = \sum_i \left(\hat{K}_i + \hat{U}_\iota\right) + \sum_i \left(\sum_j \hat{V}_{ij} - \hat{U}_i\right) \tag{2}$$

where the second term on the right-hand side is known as residual interaction V_{res},

$$V_{res} = \sum_{ij} \hat{V}_{ij} - \hat{U}_i. \tag{3}$$

However, Hartree-Fock assumes at the first approximation that $V_{res} \approx 0$ because the residual interaction is too small and can be neglected. So, the final equation of Hamiltonian is written as

$$\widehat{H} \approx \sum_{i}^{N} h_i^{(s.p)} \tag{4}$$

where $h_i^{(s.p)}$ is a single-particle Hamiltonian of one body interaction. But, V_{res} still plays an important role in pairing part. Hence, the pairing correlation in this study is treated in BCS scheme which approximated by the Seniority force within Skyrme energy functional (see Appendix A).

Two-neutron Separation Energy

One of the quantities of interest in our work is the two-neutron separation energy [18]. The two-neutron separation energy S_{2n} is calculated using

$$S_{2n}(N,Z) = BE(N-2,Z) - BE\,(N,Z), \tag{5}$$

where $BE(N-2,Z)$ is the binding energy from our SHF+BCS calculation for a nucleus with Z protons and N neutrons. Traditionally, the S_{2n} provides and indication on the existence of a shell gap through a large dip in the plot of S_{2n} vs N. However, another option to draw out this information in a more vivid manner is to consider the two-neutron separation energy differential ΔS_{2n} defined as

$$\Delta S_{2n}(N,Z) = S_{2n}(N,Z) - S_{2n}(N+2,Z), \tag{6}$$

as considered for e.g., in the recent work of [19].

Alpha-Decay Half-lives

Another quantity of interest is the alpha-decay half-life. We have considered various empirical formula to compute the alpha-decay half-life whereby the input for the formula is the energy released in the alpha-decay process Q_α calculated using

$$Q_\alpha = BE_{HF}(d) + BE_\alpha - BE_{HF}(p), \tag{7}$$

where $BE_{HF}(p)$ and $BE_{HF}(d)$ are the binding energies obtained from the SHF+BCS calculation for the parent nucleus and daughter nucleus, respectively. The binding energy of the alpha particle, BE_α is obtained from National Nuclear Data Center (NNDC) with a value of 28.30 MeV [20].

The Viola-Seaborg formula

One of the formulae for alpha-decay half-life calculations is the Viola-Seaborg formula [21] which is based on the Gamow model. The logarithm half-life is represented by:

$$\log_{10} T_{1/2} = (aZ+b){Q_\alpha}^{-\frac{1}{2}} + cZ + d + h_{log}, \tag{8}$$

where a, b, c, and d are adjustable parameters while the quantity h_{log} is the hindrance factor for nucleus with unpaired nucleons. We considered three different sets of parameters namely VSS1 proposed by Sobiczewski *et al.* [22] in 1989, VSS2 proposed by Parkhomenko and Sobiczewski [23] in 2005 and VS3 proposed by Dong and Ren [24] in 2005. The parameter constants can be

found in the Table 1. In this study, even-even nuclei are chosen and the value of h_{log} for even-even nuclei is zero.

TABLE 1: List of parameter constants of VSS1, VSS2 and VS3.

	VSS1 [22]	**VSS2** [23]	**VS3** [24]
a	1.66175	1.3892	1.64062
b	-8.5166	13.862	-8.54399
c	-0.20228	-0.1086	-0.19430
d	-33.9069	-41.458	-33.9054

Brown and modified Brown formula

The empirical Brown formula is given by

$$\log_{10} T_{1/2} = a(Z-2)^b Q_\alpha^{-1/2} - c + h^{mb1}, \quad (9)$$

where a, b, and c are adjustable parameters. Different parameters are also used for this formula namely BF proposed by Brown in 1922 [25], and mB1 and mB2 proposed by Budaca *et al.* [26] in 2016. The value for h^{mb1} are zero for even-even nuclei case. The parameter constants are listed in the Table 2.

TABLE 2: List of parameter constants of BF, mB1 and mB2.

	BF [25]	**mB1** [26]	**mB2** [26]
a	9.54	13.0705	10.8238
b	0.6	0.5182	-47.8867
c	-51.37	-47.8867	-56.9785

iii. Royer Formula

The Royer formula was proposed by Royer [27] in 2002 and is written as

$$\log_{10} T_{1/2} = -a - bA^{\frac{1}{6}}\sqrt{Z} + \frac{cZ}{\sqrt{Q_\alpha}}, \quad (10)$$

where a, b, and c are adjustable parameters fixed as a = 25.31, b = 1.1629, and c = 1.5864 in Ref [27].

TECHNICAL DETAILS

In this study, the SkM* [28] parametrization is used for the effective nucleon-nucleon interaction part, while the residual pairing interaction entering the BCS calculation is approximated by the seniority force. The pairing matrix element using the seniority force is written as

$$V_{k\tilde{k}l\tilde{l}} = \langle k\tilde{k}|V_p|l\tilde{l}\rangle = \frac{G_q}{11 + N_q}\ MeV, \tag{11}$$

where G_q and N_q is the pairing strength and the number of nucleons associated with the charge state q, respectively. We considered two set of pairing strengths which are

- G_n= 16.0 MeV, G_p= 16.0 MeV based on the work of [29]
- G_n and G_p fitted to reproduce the Madland pairing gap equations [30].

For the second option, we adjust the pairing strengths to fit the BCS pairing gap to the empirical Madland pairing gap given as:

$$\bar{\Delta}_n = r\ exp\frac{-sI - tI^2}{N^{1/3}}, \tag{12}$$

$$\bar{\Delta}_p = r\ \exp\frac{sI - tI^2}{Z^{1/3}}, \tag{13}$$

where $I = \frac{N-Z}{A}$ is the relative neutron excess, r = 5.72 MeV, s = 0.118, t = 8.12 are constants [30]. The attempt to fit the pairing strengths via the Madland's equation was made to gauge the order of the impact brought by the choice of pairing strengths specifically on the alpha-decay half-life. A more thorough investigation is needed. For this reason, most results presented herein are based on the fixed value of $(G_n, G_p) = (16{,}16)$ MeV unless stated otherwise.

Optimization of oscillator b and deformation q parameters were performed assuming an axial and parity symmetrical nuclear shapes where $b = \sqrt{\frac{mw_0}{\hbar}}$ and $q = \frac{w_\perp}{w_z}$ in order to get the lowest energy at each deformation points in a chosen basis size N_0. In this study, basis size $N_0 = 18$ is chosen.

RESULTS

Evolution of Q_{20}

The binding energies obtained from SHF+BCS calculations at different deformation points (from -40 barn to 40 barn) are used to plot the potential energy surface for Lv- and Og-isotopes. Fig. 1 shows the potential energy surface as a function of quadrupole moments Q_{20} for (a) Lv- and (b) Og-isotopes. The dotted line at each plot is used to show where is the spherical region.

From the plot, we see that the shapes of Lv-isotopes are gradually changing from an oblate shape (in N = 174 and 176) to spherical shape as it approaches the neutron number N = 184. The ground states (not visible in the plot) for N = 182 is slightly oblate while the ground-state for N = 186 is slightly prolate. The same pattern occurs for Og-isotopes where the global minimum is located at oblate shape for N = 176 and then minimum gradually shifted towards sphericity at N = 184. The evolution of the potential energy surface for different neutron numbers indicates that N = 184 is a strong candidate as a spherical neutron magic number in this region.

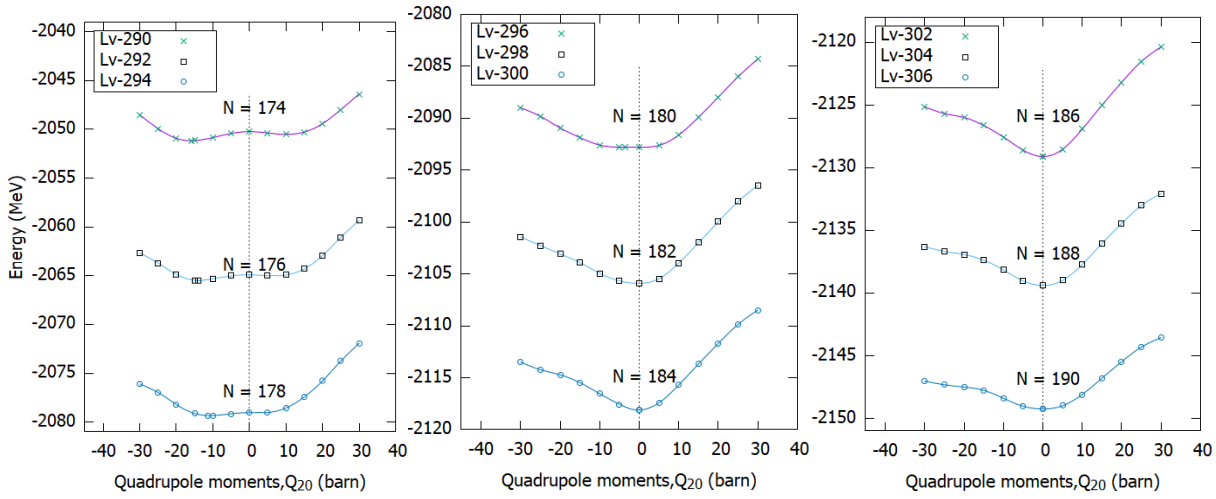

(a)

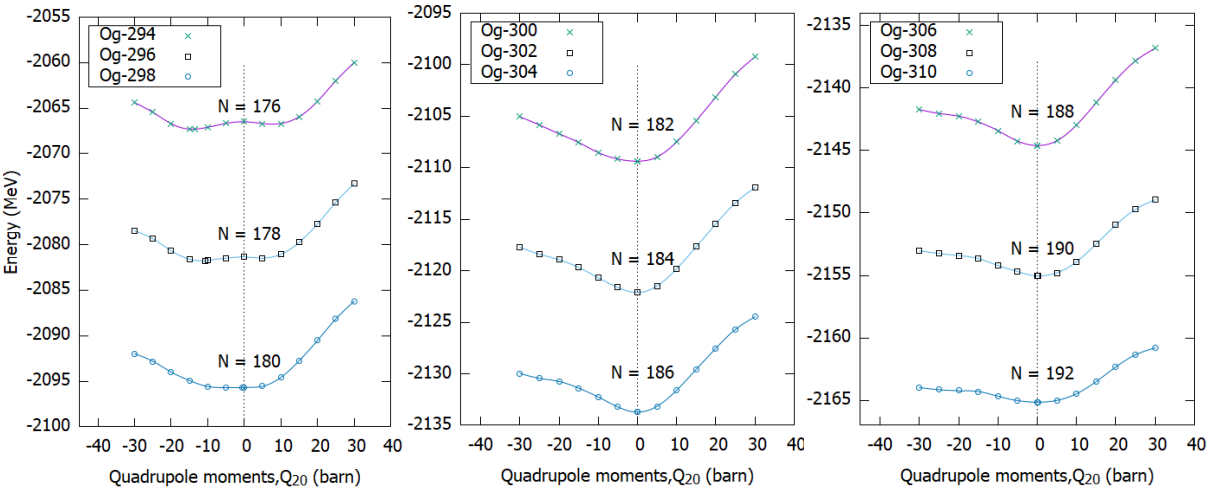

(b)

FIGURE 1. Potential energy surface of (a) Lv- and (b) Og-isotopes using (16,16) pairing strength.

Separation Energy

Fig. 2 shows the two-neutron separation energy while Fig. 3 shows the two-neutron separation energy differential, both as a function of neutron number of Lv- and Og-isotopes. For this analysis, we considered the solutions at the global minimum (Lv_{gs}, Og_{gs}) and at sphericity (Lv_{sp}, Og_{sp}) of Lv- and Og-isotopes. We see a sharp peak in the two-nucleon separation energy differential plot at N = 184 for both types of solutions. This peak confirms magicity of N = 184, which translates to a significant energy gap in the single-particle energy spectra.

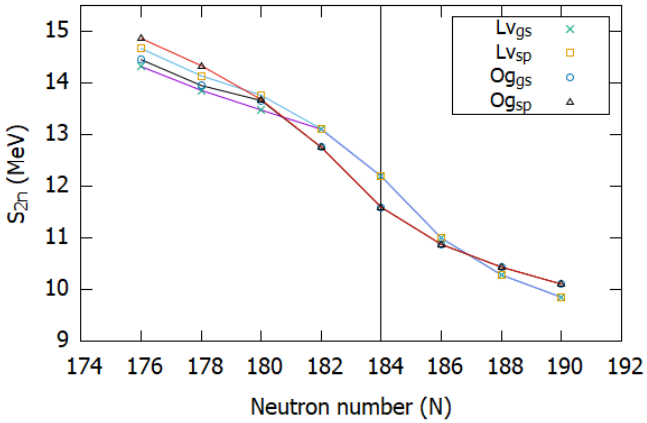

FIGURE 2. Two-neutron separation energy (S_{2n}) as a function of neutron number *N* of Lv- and Og-isotopes at the global minimum (Lv_{gs}, Og_{gs}) and at sphericity (Lv_{sp}, Og_{sp}) using (16,16) pairing strength. Black line is used to indicate the expected neutron magic number.

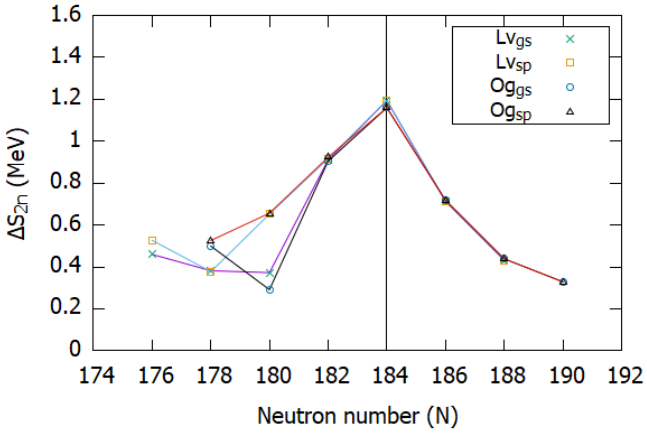

FIGURE 3. Two-neutron separation energy differential (ΔS_{2n}) as a function of neutron number *N* of Lv- and Og-isotopes isotopes at the global minimum (Lv_{gs}, Og_{gs}) and at sphericity (Lv_{sp}, Og_{sp}) using (16,16) pairing strength. Black line is used to indicate the expected neutron magic number.

Alpha Decay Half-Lives

We performed calculations of the alpha-decay half-lives using the Q_α values from the difference in binding energies of Og-isotopes (parent nuclei) and Lv-isotopes (daughter nuclei) as an input to the seven semi-empirical formulas mentioned above. The half-lives are plotted as a function of neutron number in Fig. 4(a) and Fig. 4(b) with results obtained from the ground-state solutions, and the constrained calculations at sphericity, respectively.

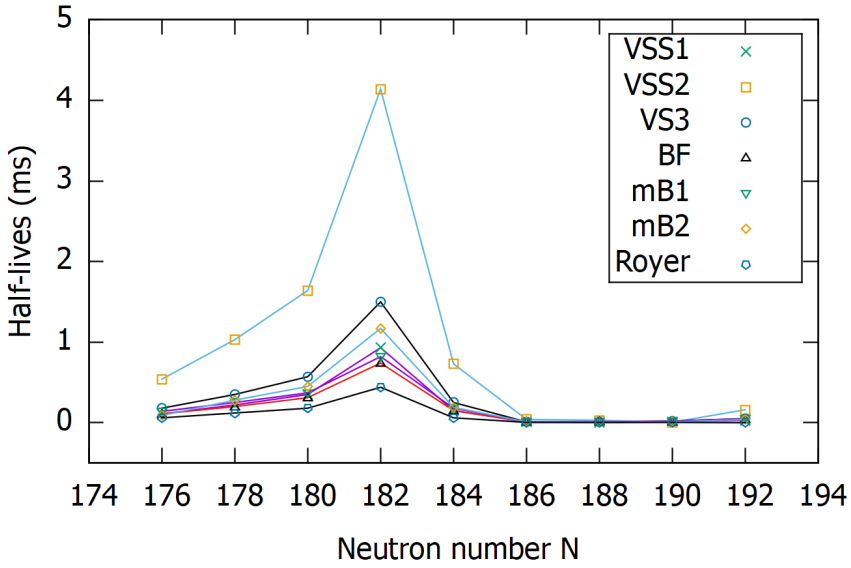

(a)

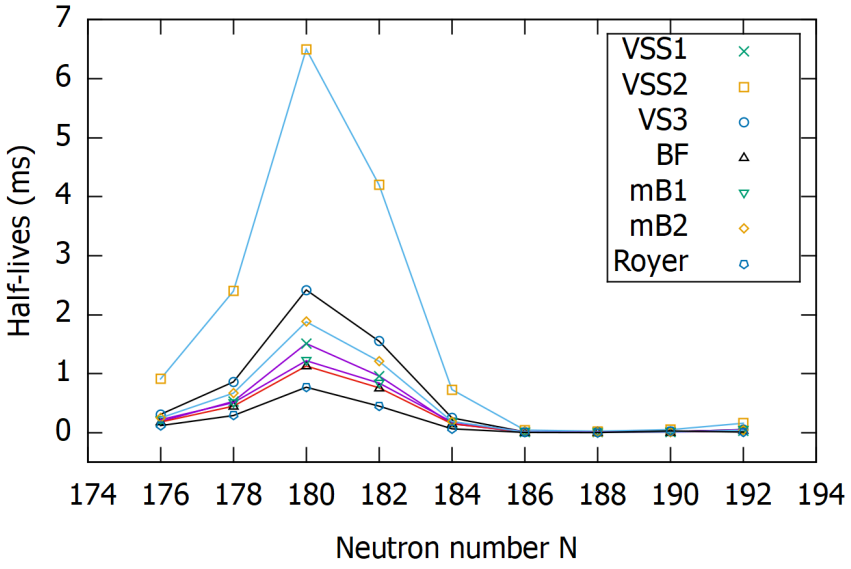

(b)

FIGURE 4. The alpha-decay half-lives as a function of neutron of Og-isotopes using (16,16) pairing strength at (a) ground-state and (b) sphericity solutions.

For the ground-state solution, all the semi-empirical formulas gave a peak at $N = 182$, indicating that the ^{300}Og (with 182 neutrons) is the most stable isotope in the considered Og chain. On the other hand, the peak in the half-life plot shifted to $N = 180$ when we consider the solution at spherical shape. In both cases, the half-lives predicted using the VSS2 formula accentuates the peak as compared to other formula.

One important factor in the BCS part of the calculation is the determination of pairing strengths. In this work, we compare the alpha-decay half-life obtained with pairing strengths obtained with

two different approaches for the ground-state of ^{294}Og nucleus. One is with a fixed (16,16) pairing strengths and another is where the pairing strengths are adjusted to reproduce the Madland pairing gap at the ground-state deformation. The results are tabulated in Table 3. Based on the comparison with experimental data, we found that the choice of a fixed pairing strengths of (16,16) underestimates the alpha-decay half-life for all formulas except for the VSS2 whereby the calculated value is just barely within the experimental error bar. On the contrary, adjusting the pairing strengths to the Madland pairing gap give results which are close to the upper limit of the experimental data for BF, mB1, mB2 and Royer formula, while overestimating the half-life for the other three formulas. These comparisons can be seen more clearly in Fig. 5.

TABLE 3: Comparison between the calculated alpha-decay half-lives obtained with a fixed pairing strength and those adjusted to reproduce Madland pairing gap. Experimental data of ^{294}Og is taken from Ref [3].

Type	Half-lives (ms)		
	(16.0, 16.0)	Madland	Experimental
VSS1	0.11	2.01	
VSS2	0.54	8.59	
VS3	0.18	3.21	$0.69^{+0.64}_{-0.22}$
BF	0.11	1.46	
mB1	0.14	1.54	
mB2	0.09	1.60	
Royer	0.06	1.22	

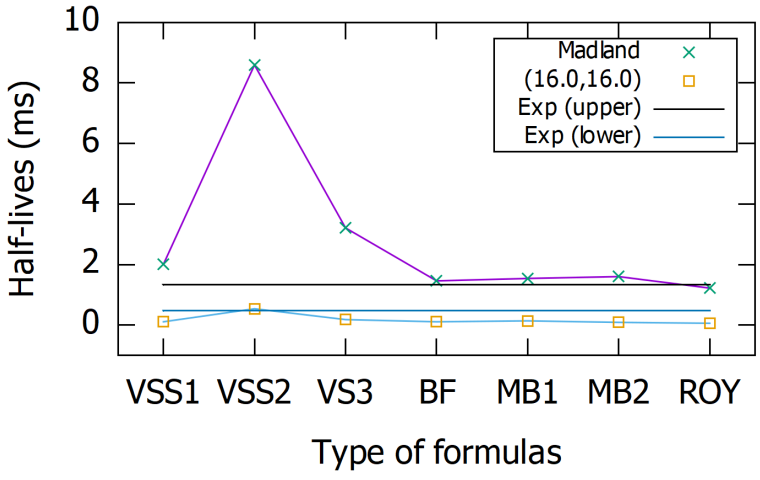

FIGURE 5. The alpha-decay half-lives of ^{294}Og calculated using seven semi-empirical formulas. The upper and lower bound of the experimental half-life were indicated by the horizontal lines.

CONCLUSION

In this paper, we present preliminary results of nuclear properties of two superheavy elements namely Lv- and Og-isotopes obtained using SHF+BCS approach. The SkM* parametrization is used in our calculations. We have shown that the potential energy surface and two-neutron separation energy differential of Lv- and Og-isotopes indicated N = 184 as a potential spherical neutron magic number. However, the peak in the alpha decay half-life appears at N = 180 and N =182 for the Og-isotopes when using the (16,16) set of pairing strength for spherical and ground-state solutions, respectively. Finally, we showed that the choice of pairing strengths has a huge impact on the alpha-decay half-life of ^{294}Og nucleus. Investigation on impact of pairing with an average pairing strength in the superheavy region is under the preparation and will be reported soon.

ACKNOWLEDGMENTS

The authors would like to acknowledge the Ministry of Education Malaysia for the financial support through the Fundamental Research Grant Scheme (FRGS/1/2018/ST/G02/UTM/02/6) and UTM (R.J130000.7854.5F028).

APPENDIX

Skyrme Energy Density Functional

A phenomenological Skyrme interaction is used whereby the expectation value of the Hamiltonian using the Skyrme interaction can be written as

$$E = \langle \psi_{HF} | \widehat{H} | \psi_{HF} \rangle = \int \mathcal{H}(r) dr = \int [\mathcal{H}_{kin}(r) + H_c(r) + \mathcal{H}_{DD}(r) + H_{SO}(r) + \mathcal{H}_{Coul}(r)] dr, \quad \text{(A1)}$$

where the kinetic energy, central, density-dependent, spin-orbit and Coulomb Hamiltonian densities are denoted as $\mathcal{H}_{kin}(r)$, $H_c(r)$, $\mathcal{H}_{DD}$, $H_{SO}(r)$ and $\mathcal{H}_{Coul}(r)$[31, 32]. The Hamiltonian densities are given below in terms of the coupling constant B_i:

$$H_{kin}(r) = \left(1 - \frac{1}{2}\right) \frac{\hbar^2}{2m} \tau, \quad \text{(A2)}$$

$$\begin{aligned} \mathcal{H}_c(r) = {} & B_1 \rho^2 + B_{10} s^2 + B_3(\rho\tau - j^2) + B_{14}(\vec{J}^2 - s \cdot T) + B_5 \rho \Delta\rho + B_{18} s \cdot \Delta s \\ & + \sum_q \left\{ B_2 \rho_q^2 + B_{11} s_q^2 + B_4\left(\rho_q \tau_q - j_q^2\right) + B_{15}\left(\vec{J}_q^2 - s_q \cdot T_q\right) \right\} \\ & + B_6 \rho_q \Delta\rho_q + B_{19} s_q \cdot \Delta s_q, \end{aligned} \quad \text{(A3)}$$

$$H_{DD}(r) = \rho^\alpha \left[B_7 \rho^2 + B_{12} s^2 + \sum_q (B_8 \rho_q^2 + B_{13} s_q^2) \right], \quad \text{(A4)}$$

$$\mathcal{H}_{SO}(r) = B_q\left[\rho\nabla\cdot J + j\cdot\nabla\times s + \sum_q\left(\rho_q\nabla\cdot J_q + j_q\cdot\nabla\times s_q\right)\right], \tag{A5}$$

$$\mathcal{H}_{Coul}(r) \approx \frac{1}{2}\rho_p(r)V_{CD}(r) - \frac{3}{4}e^2\left(\frac{3}{\pi}\right)^{\frac{1}{3}}\rho_p^{\frac{4}{3}}(r). \tag{A6}$$

s, j and T are time-odd local densities namely spin density, momentum density and kinetic energy density (vector part), respectively. While the local densities that are time-even namely particle density $\rho(r)$, kinetic energy density $\tau(r)$ and spin-current density $J_{\mu v}(r)$ depends on the single-particle wave function in the following form [31, 32]:

$$\rho(r) = \sum_k v_k^2[\phi_k]^\dagger(r)[\phi_k](r), \tag{A7}$$

$$\tau(r) = \sum_k v_k^2\left(\nabla[\phi_k]^\dagger(r)\right)\cdot\nabla[\phi_k](r), \tag{A8}$$

$$J_{\mu v}(r) = \frac{1}{2i}\sum_k v_k^2\left\{[\phi_k]^\dagger(r)\sigma_v\nabla_\mu[\phi_k](r) - (\nabla_\mu[\phi_k]^\dagger(r))\sigma_v[\phi_k](r)\right\}. \tag{A9}$$

The Hartree-Fock equations can be obtained by varying Eq. (A1) with respect to the wave-function of single-particle ϕ_k and the one-body Hamiltonian $\hat{h}_{HF}$ [31, 32] can be expressed as

$$\begin{aligned}\left\langle r\left|\hat{h}_{HF}^{(q)}\right|\phi_k\right\rangle = & -\nabla\cdot\left(\frac{\hbar^2}{2m_q^*(r)}\nabla[\phi_k](r)\right) + \left[U_q(r) + \delta_{qp}U_{Coul}(r)\right][\phi_k](r)\\ & + iW_q(r)\cdot[\sigma\times\nabla[\phi_k](r)]\\ & - i\sum_{\mu,v}\left\{\left[W_{q,\mu v}^{(J)}(r)\sigma_v\nabla_\mu[\phi_k](r)\right] + \nabla_\mu[W_{q,\mu v}^{(J)}(r)\sigma_v[\phi_k](r)]\right\}\\ & - \frac{i}{2}\left\{A_q(r)\cdot\nabla[\phi_k](r) + \nabla\cdot\left[A_q[\phi_k](r)\right]\right\} + S_q(r)\cdot\sigma[\phi_k](r) - \nabla\\ & \cdot\left\{\left[C_q(r)\cdot\sigma\right]\nabla[\phi_k](r)\right\}.\end{aligned} \tag{A10}$$

The symbol of S_q, A_q, and C_q terms vanish when the time reversal symmetry is conserved and the effective mass m^*, central-plus-density U_q, Coulomb field U_{Coul}, spin-current density $W_{q,\mu v}^{(J)}$ can be expressed as following [31, 32]:

$$\frac{\hbar^2}{2m_q^*} = \frac{\hbar^2}{2m_q} + B_3\rho + B_4\rho_q, \tag{A11}$$

$$\begin{aligned}U_q = & 2\left(B_1\rho + B_2\rho_n\right) + B_3\tau + B_4\tau_q 2\left(B_5\delta_\rho + B_6\delta\rho_q\right) + (2+\alpha)B_7\rho^{1+\alpha}\\ & + B_8\left(\alpha\rho^{(\alpha-1)}\left(\rho_n^2+\rho_p^2\right) + 2\rho^\alpha\rho_q\right) + B_9\left(\nabla\cdot J + \nabla\cdot J_q\right)\\ & + \alpha\rho^{\alpha-1}(B_{12}s^2 + S_{13}\left(s_n + s_p\right),\end{aligned} \tag{A12}$$

$$U_{Coul} = V_{dir} - e^2\left(\frac{3}{\pi}\rho_p\right)^{\frac{1}{3}}, \tag{A13}$$

$$W_q = -B_9\left(\nabla_\rho + \nabla\rho_q\right), \tag{A14}$$

$$W_{q,\mu,v} = B_{14}J_{\mu v} + B_{15}J_{q,\mu v}, \tag{A15}$$

$$S_q = 2(B_{10} + B_{12}\rho^\alpha)s + 2(B_{11} + B_{13}\rho^\alpha)s_q - B_9\nabla\times\left(j + j_q\right) - B_{14}T - B_{15}T_q + 2\left(B_{18}\Delta s + B_{19}s_q\right), \tag{A16}$$

$$A_q = -2\left(B_3 j + B_4 j_q\right) + B_9\nabla\times\left(s + s_q\right), \tag{A17}$$

$$C_q = -\left(B_{14}s + B_{15}s_q\right). \tag{A18}$$

REFERENCES

1. Y. T. Oganessian et al., Phys. Rev. C **74**, 044602 (2006).
2. M. G. Mayer, Phys. Rev. C **74**, 235-239 (1948).
3. Y. T. Oganessian and V. Utyonkov, Nucl. Phys. A **944**, 62-98 (2015).
4. J. L. Egido and A. Jungclaus, Phys. Rev. Lett. **125**, 192504 (2020).
5. K. P. Santhosh and C. Nithya, Phys. Rev. C **97**, 044615 (2018).
6. O. Nagib, Phys. Rev. C **101**, 014610 (2020).
7. P. Sarriguren, Phys. Lett. B **815**, 136149 (2021).
8. Z. Ge, G. Zhang, S. Cheng, Y. Li, N. Su, W. Guo, Y. S. Tsyganov, and F.-S. Zhang, Eur. Phys. J. A **55**, 166 (2019).
9. X. J. Bao, S. Q. Guo, H.F. Zhang, and J. Q. Li, Phys. Rev. C **95**, 034323 (2017).
10. A. Fabrocini, "A Microscopic Approach to Nuclear Physics: from Deuteron to Neutron Stars" *Recent Developments in General Relativity*, Milan: Springer, 2000, pp. 71–86.
11. V. Strutinsky, Nucl. Phys. A **95**, 420-442 (1967).
12. M. Bender, K. Rutz, P.-G. Reinhard, J.A. Maruhn, and W. Greiner, Phys. Rev. C **60**, 034304 (1999).
13. S. Cwiok, W. Nazarewicz, and P.H Heenen, Phys. Rev. Lett. **83**, 1108-1111 (1999).
14. Y. T. Oganessian *et al.*, Phys. Rev. C **72**, 034611 (2005).
15. Z. Patyk and A. Sobiczewski, Nucl. Phys. A **533**, 132-152 (1991).
16. A. T. Kruppa, M. Bender, W. Nazarewicz, P.-G. Reinhard, T. Vertse, and S. Cwiok, Phys. Rev. C **61**, 034313 (2000).

17. A. Baran, Z. Łojewski, K. Sieja and M. Kowal, Phys. Rev. C **72**, 044310 (2005).
18. K.S. Krane, D. Halliday *et al.*, *Introductory Nuclear Physics*, New York: John Wiley & Sons, (1988).
19. K.-W. Kelvin-Lee, M.-H. Koh, and L. Bonneau, Phys. Rev. C **103**, 064315 (2021).
20. A. Sonzogni, "Interactive Chart of Nuclides", National Nuclear Data Center: Brookhaven National Laboratory (2008).
21. V.E. Viola and G.T. Seaborg, J. Inorg. Nucl. Chem. **28**, 741 (1966).
22. A. Sobiczewski, Z. Patyk, and S. Cwiok, Phys. Lett. B **224**, 1 (1989).
23. A. Parkhomenko and A. Sobiczewski, Acta Phys. Pol. B **36**, 3095 (2005).
24. T. Dong and Z. Ren, Eur. Phys. J. A **26**, 69 (2005).
25. B. A. Brown, Phys. Rev. C **46**, 811 (1992).
26. A. I. Budaca, R. Budaca, and I. Silisteanu, Nucl. Phys. A **951**, 60 (2016).
27. G. Royer, J. Phys. G **26**, 1149 (2000).
28. J. Bartel, P. Quentin, M. Brack, C. Guet, and H.-B. Hakansson, Nucl. Phys. A **386**, 79-100 (1982).
29. M.-H. Koh, L. Bonneau, P. Quentin, T. V. N. Hao, and H. Wagiran, Phys. Rev. C **95**, 014315 (2017).
30. D. G. Madland and J. R. Nix, Nucl. Phys. A **476**, 1 (1988).
31. Y. M. Engel, D. M. Brink, K. Goeke, S. J. Krieger, and D. Vautherin, Nucl. Phys. A **249**, 215 (1975).
32. P. Bonche, H. Flocard, and P.H. Heenen, Nucl. Phys. A **467**, 115 (1987).